Changes in brain perfusion in successive arterial spin labeling MRI scans in neonates with hypoxic-ischemic encephalopathy

Maïa Proisy[a,b,*], Isabelle Corouge[a], Antoine Leghouy[a], Amélie Nicolas[b], Valérie Charon[b], Nadia Mazille[c], Stéphanie Leroux[c], Bertrand Bruneau[b], Christian Barillot[a], Jean-Christophe Ferré[a,b]

[a] Univ Rennes, Inria, CNRS, INSERM, IRISA, Empenn ERL U-1228, F-35000 Rennes, France
[b] CHU Rennes, Radiology Department, F-35033 Rennes, France
[c] CHU Rennes, Neonatology Department, F-35033 Rennes, France

ARTICLE INFO

ABSTRACT

The primary objective of this study was to evaluate changes in cerebral blood flow (CBF) using arterial spin labeling MRI between day 4 of life (DOL4) and day 11 of life (DOL11) in neonates with hypoxic-ischemic encephalopathy (HIE) treated with hypothermia. The secondary objectives were to compare CBF values between the different regions of interest (ROIs) and between infants with ischemic lesions on MRI and infants with normal MRI findings.

We prospectively included all consecutive neonates with HIE admitted to the neonatal intensive care unit of our institution who were eligible for therapeutic hypothermia. Each neonate systematically underwent two MRI examinations as close as possible to day 4 (early MRI) and day 11 (late MRI) of life. A custom processing pipeline of morphological and perfusion imaging data adapted to neonates was developed to perform automated ROI analysis.

Twenty-eight neonates were included in the study between April 2015 and December 2017. There were 16 boys and 12 girls. Statistical analysis was finally performed on 37 MRIs, 17 early MRIs and 20 late MRIs. Eleven neonates had both early and late MRIs of good quality available. Eight out of 17 neonates (47%) had an abnormal on late MRI as performed and 7/20 neonates (35%) had an abnormal late MRI. CBF values in the basal ganglia and thalami (BGT) and temporal lobes were significantly higher on DOL4 than on DOL11. There were no significant differences between DOL4 and DOL11 for the other ROIs. CBF values were significantly higher in the BGT vs. the cortical GM, on both DOL4 and DOL11. On DOL4, the CBF was significantly higher in the cortical GM, the BGT, and the frontal and parietal lobes in subjects with an abnormal MRI compared to those with a normal MRI. On DOL11, CBF values in each ROI were not significantly different between the normal MRI group and the abnormal MRI group, except for the temporal lobes.

This article proposes an innovative processing pipeline for morphological and ASL data suited to neonates that enable automated segmentation to obtain CBF values over ROIs. We evaluate CBF on two successive scans within the first 15 days of life in the same subjects. ASL imaging in asphyxiated neonates seems more relevant when used relatively early, in the first days of life. The correlation of intra-subject changes in cerebral perfusion between early and late MRI with neurodevelopmental outcome warrants investigation in a larger cohort, to determine whether the CBF pattern change can provide prognostic information beyond that provided by visible structural abnormalities on conventional MRI.

1. Introduction

Hypoxic-ischemic encephalopathy (HIE) is the leading cause of neonatal encephalopathy and occurs after perinatal asphyxia in full-term neonates. HIE is a major cause of perinatal mortality and morbidity (Volpe, 2012). MRI plays a key role in the diagnosis and

prognosis of this pathology. The time to perform MRI varies by center and there is no consensus on optimal timing. An early MRI (performed during the first week of life) reliably detects severe injuries and there is good agreement between early MRI and late MRI (after 1 week) (Agut et al., 2014; Boudes et al., 2015; Chakkarapani et al., 2016; Charon et al., 2015; Skranes et al., 2015). In addition to MRI scoring, some quantitative biomarkers such as DWI with measurements of apparent diffusion coefficient (ADC) or proton MR spectroscopy could contribute to an early diagnosis and prognosis (Alderliesten et al., 2011; Cheong et al., 2006). The brain perfusion model and its relationship to other biomarkers could help guide the development of therapies in order to improve management of high-risk neonates.

Cerebral perfusion imaging is challenging in neonates due to physiological and technical issues (Proisy et al., 2016). The Arterial Spin Labeling (ASL) MRI perfusion sequence is one of the most suitable imaging modalities owing to its non-invasive and non-irradiating nature. Moreover, this perfusion imaging sequence can be easily incorporated into standard brain MRI in neonates with HIE, after acquisition of morphological images. However, the post-processing of ASL data requires specific adaptations to this age group, in particular with respect to the automated segmentation of brain tissues and the parameters used for the quantification models of cerebral blood flow (CBF) (Varela et al., 2015).

There are a dozen articles in the literature concerning the study of cerebral perfusion in neonates using ASL, four of which are focused on neonates with HIE. Brain perfusion measurement may vary according to the timing of the MRI scan. Regarding the MRI time point for the studies (ranging from day 1 of life (DOL1) to the second week of life), some of the studies showed brain hyperperfusion in infants with HIE (De Vis et al., 2015; Pienaar et al., 2012), while others showed hypoperfusion (Massaro et al., 2013). In one study (Wintermark et al., 2011), two successive MR images were taken of each asphyxiated neonate during the first week of life. On DOL1, hypoperfusion was found in the brain areas subsequently exhibiting injury in the neonates treated with hypothermia and who developed MR imaging evidence of HIE brain injury. On DOL2, the CBF values were higher in the injured brain areas in these neonates. Moreover, De Vis et al. (De Vis et al., 2015) showed good performance for ASL in predicting outcome after HIE. ASL perfusion in the basal ganglia and thalami was higher in the adverse outcome group than in the favorable outcome group.

The primary objective of our study was to evaluate the changes in CBF between an early MRI (at day 4 of life) and a late MRI (at day 11 of life) in infants with HIE treated with hypothermia. The secondary objectives were to compare CBF values between the different regions of interest (ROIs) and between infants with ischemic MRI lesions and those with normal MRI.

2. Materials and methods

2.1. Patients

This prospective study included all consecutive neonates with HIE admitted to the neonatal intensive care unit of our institution between April 2015 and December 2017. The criteria of national guidelines (Saliba and Debillon, 2010) were used to determine eligibility for therapeutic hypothermia. All included neonates were at least 36 weeks' gestation with birth weight ≥ 1800 g. They had signs of perinatal asphyxia with an acute perinatal event (such as severe foetal heart rate abnormalities, cord prolapse or placental abruption) and at least one of the following criteria: APGAR score ≤ 5 at 10 min; mechanical ventilation or intubation at 10 min after birth; metabolic acidosis, including cord, arterial, venous or capillary blood pH < 7 or base deficit ≥ 16 mmol/L or lactate ≥ 11 mmol/L within 60 min of birth. Neonates with stroke, congenital malformation or metabolic disorders were not included. Hypothermia was induced within 6 h after birth and continued for 72 h, with a target temperature of 33–34 °C.

The institutional medical ethics review board approved the study and parental consent was obtained.

2.2. MR acquisition

Each included neonate systematically underwent two MRI scans as follows: an early MRI performed as close as possible to day 4 of life (DOL4) and a late MRI performed as close as possible to day 11 of life (DOL11). The early MRI was performed after rewarming, at the end of hypothermia treatment. The conventional MRI scans were acquired first then ASL images were acquired at the end.

All MRI scans were acquired using a Siemens 1.5 T Magnetom Aera scanner (Siemens; Erlangen, Germany) with a 20-channel head/neck coil.

The neonates received no additional medication for the imaging study. Ventilated infants were sedated with morphine and midazolam. Spontaneously breathing infants were not sedated and were fed before the MRI scan and wrapped with a "vacuum immobiliser".

The brain MRI protocol included routine sequences as follows: 3D T1-weighted (T1w) images acquired in the sagittal plane (TR/TE = 2090/4.9 ms; resolution = $1 \times 1 \times 1$ mm^3); axial, sagittal and coronal T2-weighted (T2w) turbo spin-echo images; axial gradient-echo T2-weighted and axial DWI with b values of 0 s/mm^2 and 1000s/mm^2. Apparent diffusion coefficient (ADC) maps were automatically generated.

The perfusion 2D pulsed ASL MRI sequence used was PICORE Q2TIPS (Luh et al., 1999). Imaging parameters were as follows: TR/TE/TI1/TI2 = 3500/12/700/2000 ms; in-plane resolution = 4×4 mm^2; slice thickness = 8 mm; gap = 2 mm; 9 slices; 30 label/control pairs; total scan time = 3 min 39 s. The first volume of the ASL series was used as the M0 reference image.

2.3. Processing of imaging data

We developed a specific processing pipeline, adapted to neonatal data, for both anatomical and perfusion images in order to estimate average CBF values over the grey matter of a set of regions of interest (ROIs). The anatomical processing of our neonate images included brain extraction, reorientation and brain tissue segmentation. Our ROIs were derived from a custom anatomical atlas we built from ALBERTs data (Gousias et al., 2012). The processing of perfusion ASL images leads to a quantitative CBF map for each subject and at each time point. Combined with anatomical segmentations, this quantitative map yields CBF statistics in our ROIs. An overview of the processing pipeline is given in Fig. 1.

2.3.1. Processing of anatomical data
2.3.1.1. Construction of custom atlas. As mentioned above, we first built a custom anatomical atlas from ALBERTs data (available at http://brain-development.org/brain-atlases/neonatal-brain-atlas-albert/). The ALBERTs data consist of 20 neonate brain T1w and T2w images with associated manual delineation of 50 regions. As shown in Fig. 2, our customised atlas was based on an amended version of the method developed by Guimond et al. (2000). It takes into account both overall changes and local deformations to provide an unbiased atlas up to a rigid transformation (code available in Anima-Script[1]). The registration process used in atlas creation involves two steps: an affine registration step followed by a diffeomorphic one, both using block-matching algorithms (Commowick et al., 2012b, 2012a) available in Anima.[2]

This method produces an average neonatal brain from the ALBERTs

---
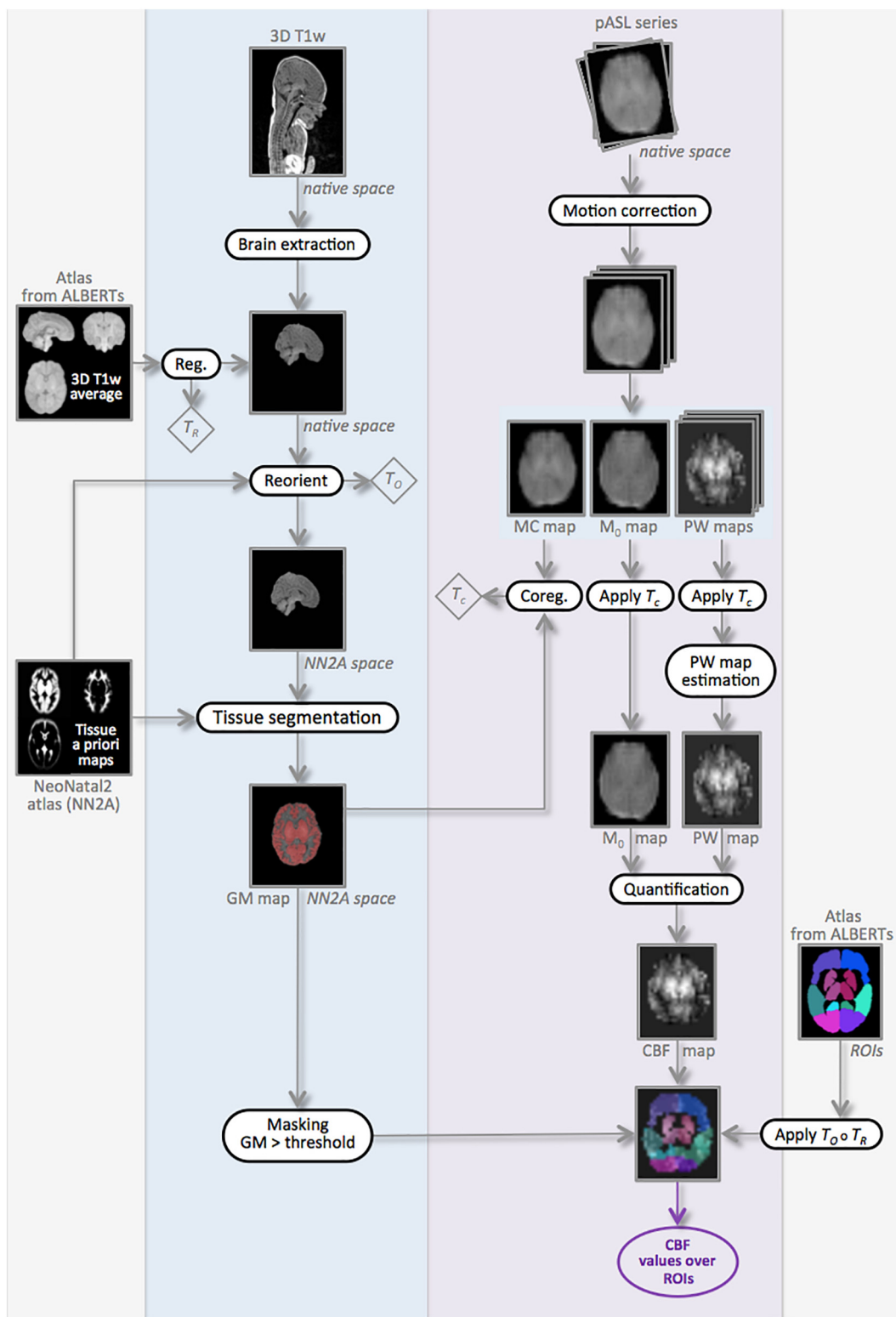
Fig. 1. Overview of our processing pipeline illustrated in one subject, at day of life 4 (DOL4). The transformations T_R, T_O and T_C resulting from the different registration steps are indicated in diamonds. The circle symbol represents the composition of transformations.

T1w images. To obtain the 50 associated segmentations, we applied the same transformation as between the individual T1w and the average T1w to the ROI map and fused the labels by majority voting. Last, for brain extraction purposes, we created a whole-brain mask by merging all the labels and applying special closing (dilation followed by hole filling and erosion).

In addition, we selected and merged subsets of ROIs from the 50 segmentation map in order to form the regions in which the CBF analysis would be performed. They are: the frontal, temporal, parietal and occipital lobes, and the basal ganglia and thalamus (BGT) for the left and right hemispheres. A "cortical GM" ROI was additionally defined as the union of the four lobes in order to obtain values for cortical GM
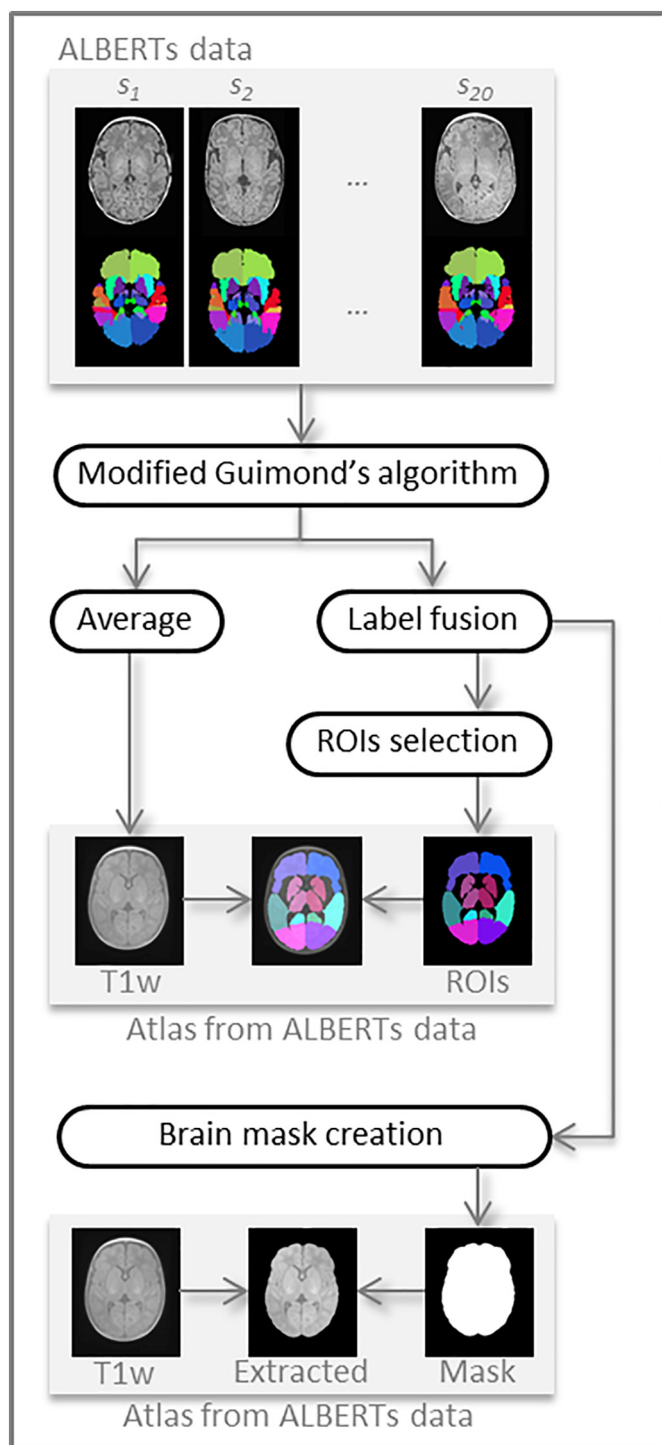
Fig. 2. Steps of the construction of our custom atlas from ALBERTs data (20 neonate subjects along with 50 manually drawn ROIs). Our custom atlas results in an average T1w image with associated ROIs, as well as an extracted average brain and a binary brain mask.

without BGT.

2.3.1.2. Brain extraction. For each subject's DOL4, the first step of anatomical processing was brain extraction. This processing is illustrated in Fig. 3. As ALBERTs and our own data show massive differences in the field of view (FOV), it was neither straightforward nor appropriate to perform brain extraction directly from the whole-brain mask computed above. We first had to crop our data to make them

compatible with ALBERTs. For this purpose we used another in-house atlas built according to the previously depicted method, but from 18 subjects selected from our neonate 3D T1w image database — so with a similar FOV — along with their associated segmentations manually drawn by a junior radiologist (AN) at our institution. These segmentations, though not as fine as those of ALBERTs, still allowed us to extract regions common to both atlases, the largest one being the cerebrum. By computing the rigid transformation between the two cerebrums, the in-house atlas could be cropped according to the ALBERTs FOV. We then propagated this desired FOV by computing another rigid transformation, T_s, this time between the in-house atlas and the subject, which enabled cropping of the subject image.

The custom atlas we built from ALBERTs data could then be registered onto our subject using an affine transformation T_A followed by a diffeomorphism transformation T_M to perform brain extraction using the whole-brain mask.

Henceforth, we will only consider the extracted brain of our subjects.

2.3.1.3. Reorientation and tissue segmentation. The extracted brain was segmented into grey matter (GM), white matter (WM) and cerebrospinal fluid (CSF) probability maps using the SPM8 toolbox (Wellcome Department of Imaging Neuroscience, University College London, London, UK). Instead of using the default SPM8 template (MNI ICMB152) tissue probability maps as an a priori for brain tissue classification, we chose the "Neonatal2 atlas — 44 weeks old, postmenstrual" (NN2 atlas) available at http://brain-development. org/brain-atlases/consistent-high-definition-spatio-temporal-neonatal-brain-atlas/, which is age-adapted to our population (Serag et al., 2012). Note that we defined the grey matter a priori probability map as the sum of the NN2 atlas cortex, deep grey matter, brainstem and cerebellum maps. The quality of the segmentation was visually checked.

Beforehand, as the data and the a priori maps needed to be roughly aligned to ensure correct segmentation with SPM8, the extracted brain was reoriented by a rigid transformation T_O onto the NN2 atlas using Anima software (Commowick et al., 2012a).

2.3.1.4. Processing of DOL11 anatomical data. Similarly to DOL4 data, the DOL11 3D T1w data first underwent brain extraction. Then, using Anima, the DOL11 image was coregistered to the DOL4 time point with an affine registration to recover the slight yet non-negligible changes due to brain growth over this period. Reorientation could then be done using the transformation computed for DOL4 before performing segmentation into brain tissues as described above.

2.3.2. Processing of perfusion data

The ASL images for all subjects and all time points were processed using a custom-built ASL pipeline based on SPM8 software and Matlab® (The MathWorks, Inc.).

The native ASL series was first visually inspected in order to detect too-large motion and perform manual suppression of control/label pairs where appropriate. It was then motion-corrected by a rigid body transformation minimising the sum of squared differences cost function. A two-pass procedure first realigned all the control and label volumes onto the first volume of the series, and then registered the series to the mean of the images aligned in the first pass.

Leaving aside the first volume of the series, M0, the ASL images were pairwise subtracted to produce a series of perfusion-weighted maps. Along with the M0 map, this series was coregistered to the 3D T1w image (once brain-extracted and reoriented) using a rigid transformation T_C. The latter was estimated by maximising normalized mutual information between the mean control image, i.e. the average of all the realigned control volumes and the 3D T1 GM map.

The perfusion-weighted (PW) map is usually obtained by averaging across the repetitions. However, as the conventional arithmetic mean is
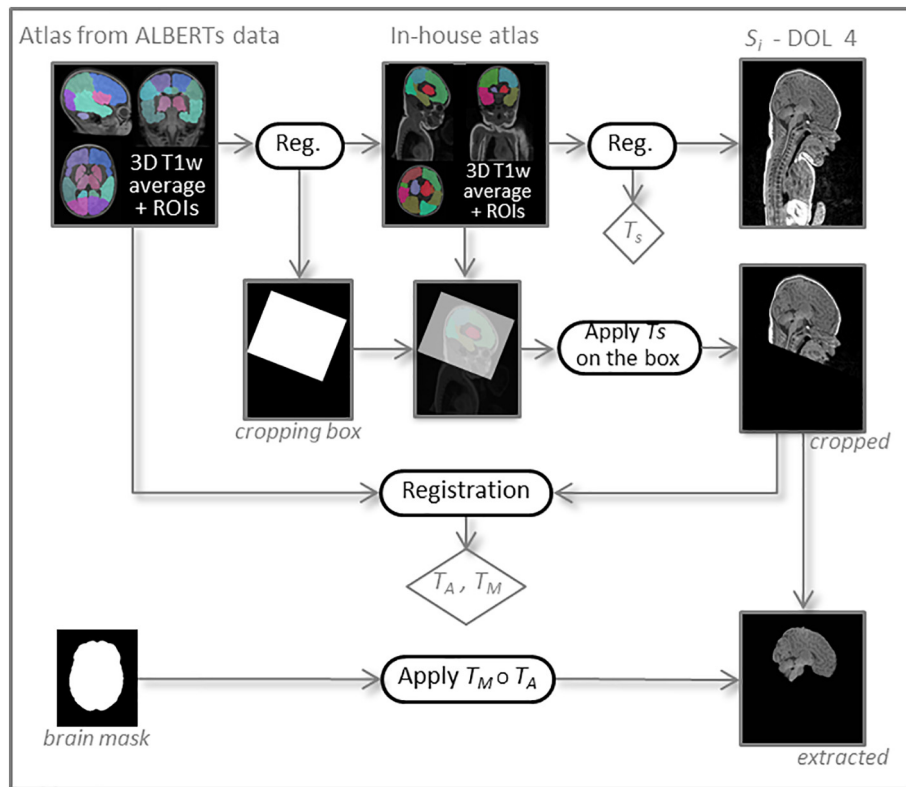
Fig. 3. Processing steps for brain extraction. The transformations T_S, T_A and T_M resulting from the different registration steps are indicated in diamonds. The circle symbol represents the composition of transformations.

very sensitive to outliers, we instead used Huber's M-estimator to robustly estimate the PW map (Maumet et al., 2014).

This robust PW map was eventually converted into a quantitative ASL CBF map by applying the standard kinetic model (Buxton et al., 1998; Wong et al., 1998)

$$\text{CBF} = 6000 \cdot \frac{\lambda \Delta M \times e^{\frac{TI_2 + idx_{sl} \times TI_{sl}}{T_{1b}}}}{2\alpha TI_1 M_{0b}} \; [\text{mL/100\,g/min}]$$

where the factor 6000 converts the unit from mL/g/s to mL/100 g/min. The labeling efficiency α was assumed to be 98% and the blood/tissue water partition coefficient λ to be 0.9 mL/g (Alsop et al., 2015). ΔM is the PW map. $TI_1 = 700$ ms is the temporal width of the bolus. TI_2, inversion time, is the time from the initial pulse to image acquisition (2000 ms). TI_2 is adjusted for each slice to take into account the time interval TI_{sl} (47 ms) between slice acquisitions in our 2D multislice ASL sequences. idx_{sl} is the slice index (0 for the first slice). T_{1b} is the longitudinal relaxation time of blood that was assumed to be 1350 ms (Alsop et al., 2015). M_{0b} is the longitudinal magnetisation of blood at equilibrium and is approximated by the M0 map.

2.3.3. Calculation of CBF statistics over ROIs

ROI analysis was used to measure mean, standard deviation, min and max values of CBF. The ROI mask built from ALBERTs data was transformed to the CBF map of each subject by a composition of transformations, T_O and T_R, T_R itself being the composition of a diffeomorphism with an affine transform between our custom ALBERTs atlas and the subject brain, and T_O being the reorientation transformation toward the Neonatal2 atlas. The data were interpolated only once with a nearest-neighbour scheme. Thus, the ROI mask, the grey matter mask of the subject and the CBF map were in coregistration.

The CBF statistics were lastly computed over each ROI (the frontal, temporal, parietal and occipital lobes, the BGT and the cortical GM ROI) intersected with the voxels having a grey matter probability higher than 0.7. In addition, the CBF statistics over the whole brain (i.e. over the voxels whose tissue sum was higher than 0.85) were also computed as an overall value for perfusion.

2.4. Data analysis

2.4.1. Qualitative analysis

ASL CBF maps were rated as having good, moderate or poor image quality by MP (7 years' experience with ASL images). Images were considered as good quality when no or only minor artefacts were present. Images were considered as moderate quality when moderate artefacts were present and did not prevent image interpretation. Images were considered poor quality when marked artefacts were present or images were considered unreadable.

Two experienced pediatric radiologists (VC and MP with, respectively, 7 and 9 years' experience) scored brain injury on MRI (T1, T2 and DWI). Early and late MRIs were assessed independently. The reviewers were blinded to the ASL sequence, clinical details and outcome of the neonates but knew the age at the time of the MRI. Assessment of brain injury was based on a previously described simplified classification (Charon et al., 2015) adapted from the Barkovich system (Barkovich et al., 1998). It distinguishes between normal/subnormal MR images — including normal MRI, punctate periventricular white matter injuries (PPWMI) and watershed pattern with a Watershed (W) score ≤ 2 on the scoring system described by Barkovich et al. (single infarction or abnormal signal in anterior or posterior watershed white matter) — and abnormal MR images including a watershed pattern with W score > 2, central or diffuse patterns. The differences were resolved by consensus between the two reviewers.

2.4.2. Quality check

In addition to visual evaluation of the ASL data, we also performed an automated quality check. As the PW map may present with negative values due to the inherent low resolution and SNR of ASL, the

percentage of negative values was calculated in the whole brain, GM and WM.

2.4.3. Quantitative analysis

Quantitative (continuous) data were expressed as median [95% confidence interval] across subjects. Normality of data distribution was checked by Shapiro-Wilk tests. As the distribution of the sample was not normal for the majority of data and because of the small sample size, non-parametric tests were used. The Wilcoxon test for paired samples was used to evaluate difference between DOL4 and DOL11 for each ROI, and differences between ROIs on DOL4 and DOL11. The Mann-Whitney test for independent samples was used to evaluate differences between normal and abnormal MRI for each ROI. A p value < .05 (two-tailed probability) was considered significant. Statistical analysis was performed using MedCalc Statistical Software version 18.2.1 (MedCalc Software bvba; Ostend, Belgium; http://www.medcalc.org).

3. Results

3.1. Study population

Twenty-eight (28) neonates were included in the study between April 2015 and December 2017. There were 16 boys and 12 girls. All of them underwent the early MRI (DOL4). There was no late MRI (DOL11) for 5 neonates, due to non-availability of an ASL sequence ($n = 4$) or death of the subject before DOL11 ($n = 1$), giving 51 scans in total.

The median age of the early MRI was day of life 3.7 (range: 3–5) and that of the late MRI was day of life 10.6 (range: 9–12). The mean gestational age at birth was 39.7 weeks (range: 36.7–41.9). Blood hematocrit values were available in 25/28 subjects at DOL4 and 11/23 subjects at DOL11, and the respective means were 43% ± 6% (range: 27–58) and 38% ± 7% (range: 26–55).

3.2. MR imaging

3.2.1. Qualitative analysis and quality check

Fourteen (27%) MRIs were excluded because of poor CBF map image quality and > 20% negative values in GM. A visual scoring of 3 and a threshold set at 20% of negative values in GM were in agreement for excluding subjects. Statistical analysis was performed on 37 MRIs, specifically 17 early MRIs and 20 late MRIs. Eleven neonates had both early and late MRIs of good quality available.

Regarding the manual suppression of pairs on preliminary visual inspection, a mean of 6 label/control pairs were deleted (range [2–14]) on DOL4 in 4 neonates, and 7.4 (range [2–15]) on DOL11, in 12 neonates. Conventional MRI scoring by two experienced pediatric radiologists concluded that 8 out of 17 neonates (47%) had an abnormal early MRI and that 7 out of 20 neonates (35%) had an abnormal late MRI. Among the 11 neonates with both early and late MRI available, 5 had normal MRI, 1 had watershed involvement with a W score ≤ 2, 1 had a watershed pattern with W score > 2, 3 had a central pattern and 1 had a diffuse pattern. Among the 6 neonates who had only an early MRI available, 2 had normal MRI, 1 had PPWM involvement, and 3 had a diffuse pattern. Among the 9 neonates who had only a late MRI available, 7 had normal MRI, 1 had a watershed pattern with W score > 2 and 1 had a central pattern.

For every patient, the scoring result was the same for the early and late MRI. No patients changed groups between the two time points.

3.2.2. Quantitative analysis

The results are provided in bilateral ROIs. ROIs are illustrated in Fig. 4.

3.2.2.1. Changes in CBF values between early and late MRI. The medians of CBF means in the BGT and temporal lobes were significantly different between the early and the late MRI ($p = .0049$ and 0.042 respectively)

with higher CBF values observed at DOL4 (See Table 1). There were no significant differences between early and late MRIs for the other ROIs. Fig. 5 shows the CBF changes in the BGT for the 11 paired subjects between DOL4 and DOL11.

3.2.2.2. Comparison of CBF values between ROIs. The medians of CBF means in each ROI are summarized in Table 2 and Fig. 6. The BGT yielded the highest median CBF values at both time points. CBF values were significantly different in the BGT vs. the cortical GM, on both the early MRI ($p < .0001$) and the late MRI ($p = .0020$). There were no significant differences between the lobes except between the temporal and frontal lobes on the early MRI ($p = .0395$).

Note that no comparison vs. brain has been performed. Whole brain CBF values are shown for comparison purposes with studies in literature using ASL or other brain perfusion imaging techniques that provide overall CBF values.

3.2.2.3. CBF values in ROIs by normal vs. abnormal MRI morphology. The medians of CBF means in each ROI are summarized in Table 3 and Fig. 7. On DOL4, the median CBF was significantly different in cortical GM ($p = .0433$), BGT ($p = .0269$), frontal ($p = .0209$) and parietal lobes ($p = .0161$) in subjects with an abnormal MRI compared to those with a normal MRI. There were no significant differences between the two groups for the whole brain and the temporal and occipital lobes. On DOL11, the median CBF in each ROI was not significantly different between the normal MRI group and the abnormal MRI group, except for the temporal lobes ($p = .0357$). In addition, if we compare the difference between the medians of the normal and abnormal MRI groups on DOL4 and on DOL11, the gap between the normal and abnormal groups is reduced on day 11 compared to day 4 ($p = .0364$).

4. Discussion

The ASL MRI sequence is highly suitable for studying cerebral perfusion in neonates and is easier to implement than other techniques. However, because of less specific pipelines than in adults the post-processing of images in infants is not yet automated. Usual brain extraction and segmentation methods are not well suited for neonate subjects. This may be explained by differences in size and cortical thickness (and therefore resolution) compared to older children but the main reason is that axons are not yet fully myelinated and so the contrast is not optimal. This study provided us with the opportunity to develop a processing pipeline of morphological and ASL data suited to neonates. We were able to automatically segment our ROIs whereas in all except one study (Tortora et al., 2017) ROIs were placed manually. Automated segmentation has the advantage of being more reproducible and allowing faster processing of large amounts of data. However, visual checking of the images and segmentations obtained currently remains necessary.

In our study, CBF values in the BGT were higher at DOL4, probably due to hyperperfusion of the BGT in subjects with an abnormal MRI. Our results are consistent with the literature. Indeed an association between ischemia and perfusion has been demonstrated (Pienaar et al., 2012). In this study, the regions with decreased diffusivity showed an increase in CBF on MRIs performed between DOL0 and DOL4 in 9 children with ischemic lesions. Wintermark et al. have shown that cooled neonates with HIE have a lower CBF on DOL1 and a higher CBF on DOL2 in injured brain areas. Conversely, in neonates who were not treated with hypothermia but who developed HI brain injury, hyperperfusion was already seen on DOL1 and appeared to peak at around DOL2-3 (Wintermark et al., 2011). Another study on ASL in a cohort of 19 term asphyxiated neonates and 4 healthy controls that were scanned at least once during the first month of life (on DOL1, DOL2-3, DOL10 or DOL30) showed similar results (Boudes et al., 2014). They reported that brain perfusion and variations in cerebral blood flow values between the newborns were the highest on days 2–3 of life and in the
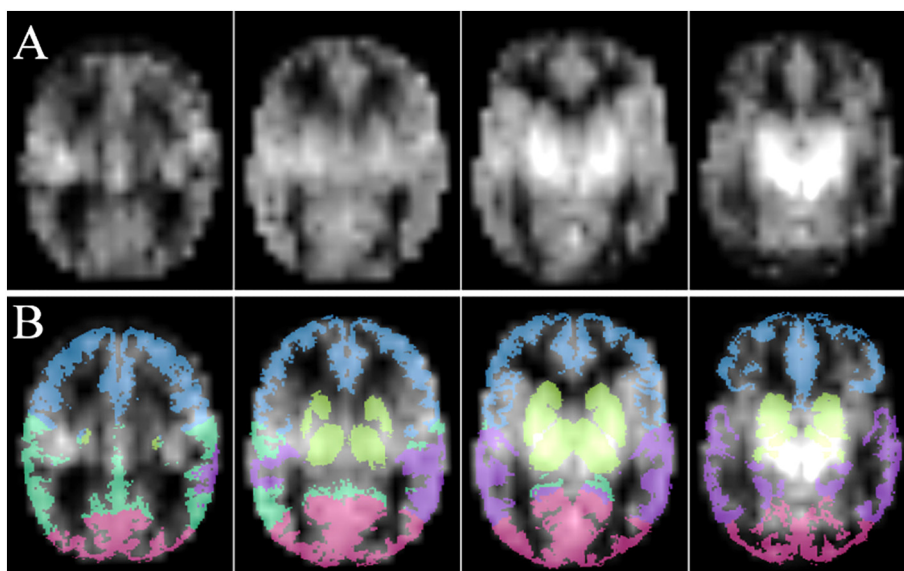
Fig. 4. Axial images of an ASL perfusion map (A) and ROI as overlay (B) with frontal (blue), parietal (dark green), occipital (pink) and temporal (purple) lobes, and basal ganglia and thalami (light green).

Table 1
Cerebral blood flow values (mL/100 g/min) in brain regions of interest, expressed as the median [95% CI].

ROI	DOL4 [n = 11]	DOL11 [n = 11]
Brain	23.8 [14.6–48.3]	19.0 [15.5–28.3]
Cortical GM	24.8 [16.3–51.6]	22.3 [15.6–37.6]
BGT	55.4 [37.8–101.2]	28.3 [19.0–47.0]**
Lobes		
Frontal	25.6 [16.2–50.3]	22.9 [13.8–39.8]
Temporal	31.5 [20.8–47.3]	23.1 [20.6–34.1]**
Parietal	25.2 [14.1–61.6]	20.7 [15.3–43.6]
Occipital	29.3 [15.5–53.7]	19.1 [15.0–36.5]

CBF = Cerebral Blood Flow; DOL4 = day 4 of life; DOL11 = day 11 of life; ROI = Region Of Interest; BGT = Basal Ganglia and Thalami; Cortical GM = Grey matter in lobes.

** Significant difference [p < .05] with the previous column [Wilcoxon test for paired sample].

asphyxiated newborns developing brain HI injury. However, no statistics reported comparison of CBF between each DOL. During the second week of life Massaro et al. found that 8 children with MRI lesions had lower CBF values in the thalamus than the children with HIE with no lesions on MRI. In contrast, children with normal MRI or watershed involvement were more likely to have hyperperfusion than controls (Massaro et al., 2013). Using dynamic susceptibility contrast (DSC) MRI, persistent cortical grey matter hyperperfusion on late scans on DOL11, instead of normalization of CBF in basal ganglia and white matter, has been reported in two term neonates with severe HI cerebral lesions (Wintermark et al., 2008).

Our study did not reveal any statistically significant differences in children with normal vs. abnormal MRI on late MRI. One explanation for this finding may be that changes in cerebral perfusion related to the ischemic perinatal insult have normalized during the second week of life. However we can observe in Table 3 and Fig. 7 that the median CBF is still higher on DOL11 in neonates with injury compared to those without. This could mean that the differences have not been found significant due to the small size of our cohort and to wide standard-deviations, as discussed below. Yet, we also observe that the gap between the normal and abnormal MRI groups – even if persisting on DOL11 - is reduced compared to DOL4. We may hypothesize that the gap will continue to diminish in the next weeks of life.

We also found hyperperfusion in the cerebral cortex (cortical GM)
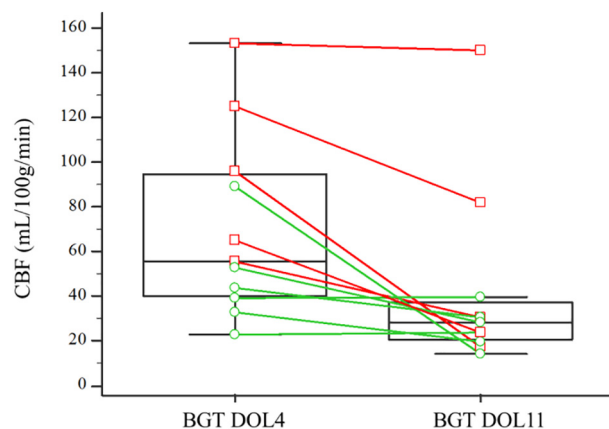
Fig. 5. Changes in cerebral blood flow in the basal ganglia and thalami for each subject (paired sample, n = 11) between day 4 and day 11 of life. The box-and-whisker plots show the lower and upper quartiles (box edges), medians (line in boxes) and minimum/maximum values (lines at ends of whiskers). The dot-and-line diagrams show infants with injury (n = 5) (red squares and lines) and without injury (n = 6) (green circles and lines) on MRI. Differences between DOL4 and DOL11 were significant (p = .049). BGT = Basal Ganglia and Thalami; CBF = Cerebral Blood Flow; DOL4 = day 4 of life, DOL11 = day 11 of life.

Table 2
Cerebral blood flow values (mL/100 g/min) in brain regions of interest, expressed as the median [95% CI].

ROI	DOL4 [n = 17]	DOL11 [n = 20]
Brain	30.5 [19.1–37.5]	21.1 [16.3–27.1]
Cortical GM	30.5 [20.8–45.0]	24.6 [18.4–32.1]
BGT	52.8 [42.6–93.6]	30.2 [24.1–48.8]
Lobes		
Frontal	25.2 [21.8–38.2]	25.1 [17.7–34.6]
Temporal	31.5 [25.4–42.1]	23.2 [21.1–30.1]
Parietal	25.8 [18.8–50.5]	23.5 [17.9–34.3]
Occipital	36.9 [19.0–51.1]	23.2 [15.9–32.6]

CBF = Cerebral Blood Flow; DOL4 = day 4 of life; DOL11 = day 11 of life; ROI = Region Of Interest; BGT = Basal Ganglia and Thalami; Cortical GM = Grey matter in lobes.
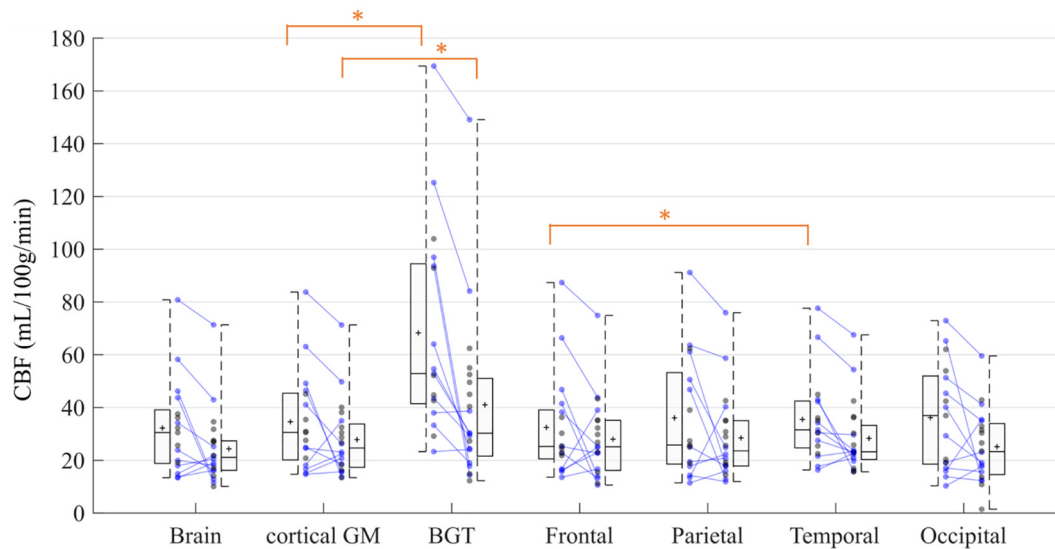
Fig. 6. Cerebral blood flow in ROIs on day 4 of life (n = 17) and day 11 of life (n = 20). Box-and-whisker plots show the lower to upper quartiles (box edges), medians (line in boxes) and minimum/maximum values (lines at ends of whiskers). The mark represents the mean. The dot-and-line diagrams (in blue) show infants with both early and late MRI (*n* = 11). The asterisk represents significant difference [p < .05] [Wilcoxon test for paired samples]. Differences between cortical GM and BGT were significant on both early and late MRI. Difference between frontal and temporal lobes was significant on early MRI. BGT = Basal Ganglia and Thalami; CBF = Cerebral Blood Flow; DOL4 = day 4 of life; DOL11 = day 11 of life; Cortical GM = Grey matter in lobes; ROI = Region Of Interest.

Table 3

Cerebral blood flow values (mL/100 g/min) in brain regions of interest by normal vs. abnormal MRI scoring. Values in ROIs are expressed as medians [95% CI].

ROI	DOL4		DOL11	
	Normal [*n* = 9]	Abnormal [*n* = 8]	Normal [*n* = 13]	Abnormal [*n* = 7]
Brain	19.9 [15.3–35.6]	35.8 [23.3–62.5]	18.0 [15.1–24.3]	26.8 [15.9–57.2]
Cortical GM	24.6 [16.8–30.8]	43.0 [25.2–66.9]*	22.3 [15.9–29.5]	32.5 [18.1–60.2]
BGT	43.4 [29.7–87.3]	80.5 [44.3–133.6]*	29.3 [17.0–42.5]	49.5 [21.0–116.9]
Lobes				
Frontal	22.7 [15.9–25.1]	37.2 [23.6–70.3]*	23.1 [14.8–30.9]	35.2 [16.7–59.4]
Temporal	30.4 [18.3–41.9]	35.1 [24.7–68.7]	22.7 [16.5–27.6]	36.2 [21.4–61.0]*
Parietal	19.4 [14.7–25.7]	55.8 [24.3–68.8]*	20.7 [16.2–32.7]	25.6 [16.9–67.4]
Occipital	20.3 [16.0–51.5]	43.9 [17.4–64.1]	19.1 [12.3–28.3]	32.9 [17.9–50.5]

CBF = Cerebral Blood Flow; DOL4 = day 4 of life; DOL11 = day 11 of life; ROI = Region Of Interest; BGT = Basal Ganglia and Thalami; Cortical GM = grey matter in lobes.

* Significant difference [p < .05] with the previous column [Mann-Whitney test for independent samples].

on early MRI in subjects with abnormal MRI. Cortical hyperperfusion is less described in the literature (Wintermark et al., 2011, 2008) and most of the studies have reported results in the BGT probably because the ROIs were manually placed, as discussed previously. The pattern of injury in asphyxiated infants is related to the type and severity of the insult. The most common pattern of injury involves the basal ganglia, but cortical involvement may be seen in infants with a chronic or repetitive insult. Given our small sample size, we were not able to perform any statistical analysis on subgroups within the abnormal MRI group. Hence, our results based on the timing of the MRI scan may not be generalized if the injury pattern distribution is different. It is, however, useful to analyze the CBF without focusing on the pattern of injury because hyperperfusion may be seen in some ROIs even if the conventional MRI does not show any injury. By way of example, one neonate in our study presented with extended cortical involvement on MRI, with relative sparing of the central grey matter seen on conventional MRI including DWI, despite having high CBF values in the BGT (125.2 mL/100 g/min on DOL4 and 84.1 on DOL11). Similarly, De Vis et al (2015) reported that one infant in their cohort had a watershed injury pattern and an adverse outcome and hyperperfusion in the BGT, indicating that hyperperfusion can occur in areas without injury on conventional MRI. Furthermore, we remark that for this subject hyperperfusion persisted on DOL11 in the BGT as well as in the cortical grey matter.

In the literature, the hyperperfusion observed on early MRI is known as the "reperfusion phenomenon" which occurs after the hypoxic ischemic event (Lassen, 1966; Pryds et al., 1990). The reperfusion phase is divided into two periods: a latent phase and an energy failure phase. The energy failure phase can occur 6 to 15 h after reperfusion and last a few days, leading to delayed cell death (Saliba and Debillon, 2010). The severity of this second phase is related to poor outcome (Batista et al., 2007; Rosenbaum et al., 1997). It still remains unclear whether hyperperfusion contributes to the injury or, on the other hand, represents a compensatory mechanism (Greisen, 2014). Wintermark et al. raised the question of the timing of the transition between the hypoperfusion phase and the hyperperfusion phase during the first days of life (Wintermark et al., 2011). Our study raises the question of the length of the hyperperfusion phase and the pattern of CBF normalization with regard to insult severity. As suggested in a previous report using DSC perfusion weighted-MRI, late hyperperfusion might represent the most severely infarcted areas taking more time to recuperate autoregulation of CBF (Wintermark et al., 2008). As an example, one neonate with a central pattern brain injury had a CBF value of 169.4 mL/100 g/min in the BGT on DOL4, which persisted on DOL11 with a value of 149.1 mL/100 g/min. This neonate had an adverse outcome and died a few days later.
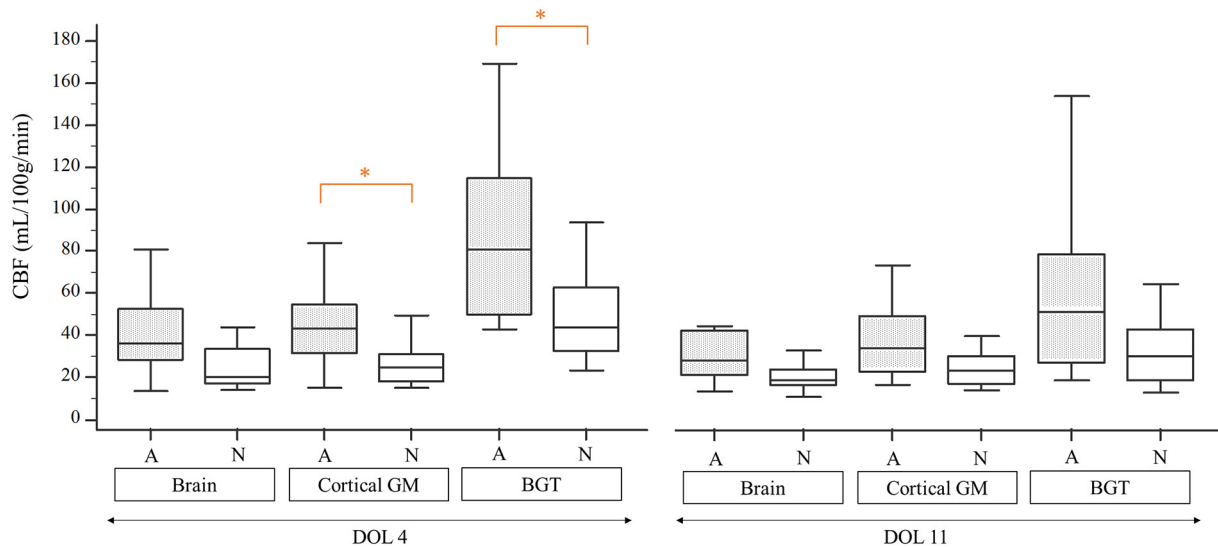
Fig. 7. Cerebral blood flow in brain, grey matter in lobes, and basal ganglia and thalami on day 4 of life for subjects with normal MRI (n = 9) vs. abnormal MRI (n = 8) and on day 11 of life for subjects with normal MRI (n = 13) vs. abnormal MRI (n = 7). Box-and-whisker plots show the lower and upper quartiles (box edges), medians (line in boxes) and minimum/maximum values (lines at ends of whiskers). Differences between infants with vs. without injury on MRI were significant (asterisk) on DOL 4 in the BGT (*p* = .0269) and in the cortical GM (*p* = .0433) [Mann-Whitney test for independent samples]. A = Abnormal MRI; BGT = Basal Ganglia and Thalami; CBF = Cerebral Blood Flow; DOL4 = day 4 of life; DOL11 = day 11 of life; Cortical GM = Grey matter in lobes; N = Normal MRI; ROI = Region Of Interest.

We found significantly higher CBF values in the BGT vs. cortical grey matter at both time points, findings that are consistent with literature data even in healthy neonates. In premature infants at term-equivalent age (TEA), De Vis et al. (2013) found CBF values of 12 ± 3 and 29 ± 9 mL/100 g/min in the whole brain and the BGT, respectively. The values reported by Miranda et al. (2006) in 6 full-term children were 16.6 ± 5.9 mL/100 g/min in the whole brain and 30.2 ± 5.5 mL/100 g/min in the BGT. There were no significant differences between the different lobes, except between the frontal and temporal lobes on DOL4. We have difficulty explaining these results and they must be interpreted with caution because of the small sample size. Moreover artefacts may be more frequent in temporal lobes because of magnetic susceptibility effects due to the air/tissue interface in mastoids. The EPI readout of the PASL sequence is known to be very sensitive to magnetic susceptibility artefacts and this could lead to perfusion measurement errors. This may also explain the isolated temporal lobe hyperperfusion in subjects with an abnormal MRI on DOL11 compared to subjects with a normal MRI. The differences in perfusion reported in literature in neonates rather concern the frontal and occipital lobes in premature infants (Ouyang et al., 2017), as seen in term-equivalent-age or healthy infants (Kim et al., 2018).

Our study has several limitations, such as, first, its low number of subjects. In common with many articles in the literature on the same topic, the frequency of the pathology and recruitment by center each year precludes large cohorts. The sample size of our study did not allow for analysis according to brain injury pattern.

The number of excluded patients is relatively high in our study (27%). The proportion of excluded patients is quite similar in the literature (around 25%) (Boudes et al., 2014; Tortora et al., 2017). The quality criteria used are variable and not detailed in the majority of the papers. Boudes et al. (Boudes et al., 2014) used a quality score developed for their study, consisting of visual analysis based on GM/WM identification and artefacts. De Vis et al. (2015) rated ASL images as having good, moderate or poor image quality by using quality criteria that included artefacts and negative voxels. We did much the same by combining visual inspection and automated measurement of voxel negatives in grey matter.

It is interesting that all the infants who were excluded did not have any motion artefacts. Understanding why the quality of the maps was

poor is crucial. One hypothesis could be that labeling failed. Acquiring ASL sequences in neonates is not as easy to achieve as in older children or adults. Indeed, in addition to the intrinsically lower SNR and resolution of the ASL sequence, the SNR is much lower in neonates because of the small size of the head and the physiologically low cerebral perfusion. An optimized PASL scheme with a restricted label volume has been proposed in order to reduced spurious negative values and intersubject variability of perfusion measurements in neonates with CHD using PASL sequences (Wang et al., 2006). Unfortunately, we were not able to reduce the labeling slab thickness (10 cm) in the acquisition parameters. This may lead to cross-contamination of the label and control acquisitions and a negative signal in the resultant perfusion images (Wang and Licht, 2006). An improvement could be expected with a pseudocontinuous ASL (pCASL) labeling scheme that was not available when we started the study on our machine. However, as shown in a study comparing PASL and pCASL (Boudes et al., 2014) to assess brain perfusion in healthy and asphyxiated newborns, the two sequences had a similar success rate. Moreover the position of the labeling slab in pCASL sequence has an impact on perfusion map and need to be adjusted for neonates. The middle of the labeling slab has to be located at the bottom of the pons instead of bottom of the cerebellum (Ouyang et al., 2017). In literature studies reporting ASL data in neonates, 8 used a PASL (Boudes et al., 2014; De Vis et al., 2015; De Vis et al., 2013; Miranda et al., 2006; Tortora et al., 2017; Varela et al., 2015; Wintermark et al., 2011, 2014) and 5 used a pCASL labeling scheme (Boudes et al., 2014; Massaro et al., 2013; Ouyang et al., 2017; Pienaar et al., 2012; Watson et al., 2016). Using a stronger magnetic field would improve the SNR but not change this proportion as all but one study (Pienaar et al., 2012) in the literature was performed using 3 T MRI scanners.

In addition, with single-TI ASL sequence, an observed signal difference might arise from a true perfusion difference as well as a difference in bolus arrival times (Buxton et al., 1998). In consequence, a lower estimated CBF might result from a longer transit time. It is known that arrival times vary across the brain and vascular territories and may be altered by pathology or low perfusion velocity (Petersen et al., 2006). In healthy adults, transit times were shown to be the shortest in caudate and putamen and the longest in the occipital area (Gallichan and Jezzard, 2009). They were also shown to differ across the lobes,

increasing from temporal to frontal, then parietal and finally occipital lobe (MacIntosh et al., 2010). However, the PASL PICORE Q2TIPS sequence used in this study is in principle insensitive to transit times as long as the timing parameters of the sequence are appropriately set (Luh et al., 1999). In particular, the inversion time should be long enough, i.e. longer than the sum of the bolus duration and transit time. Thus with appropriate timing parameters – here TI = 2000 ms as recommended in Alsop 2105 - and except in pathological cases where the transit time is lengthened, the CBF estimation should not be affected by the transit time variations.

Besides, due to the inherent low resolution of ASL, the intensity in a single voxel results from.

a mixture of the GM, WM, CSF measured signals and ASL suffers from partial volume (PV) effects. This cross-contamination between brain tissues would affect more the cortical ribbon than the deep grey nuclei leading to an underestimation of the CBF in the cerebral cortex. The cortical GM CBF values that were found lower compared to basal ganglia CBF values are possibly contributed to by this PV effect. As there is no observed difference in cortical CBF between early and late MRI while basal ganglia CBF significantly decreases from early to late MRI, the difference between cortical GM and basal ganglia values at both time points can be overestimated but not explained by cross-contamination alone. To limit cross-contamination between brain tissues, we used the "GM-threshold" approach and considered only brain voxels with GM > 0.7 in our CBF statistics computation. Nonetheless, more sophisticated methods have shown their effectiveness for PV correction in healthy adults (Petr et al., 2018). They are usually based on linear regression to estimate the CBF contribution of each tissue in every voxel. A next step would be to integrate such a method in our processing pipeline, after an evaluation of their benefit on neonatal ASL data.

As far as the quantification parameters λ and T_{1b} are concerned, we chose values from the literature. For the blood/tissue water partition coefficient λ, the current recommendation is to use a brain-averaged value (Alsop et al., 2015). Though associated quantification errors are expected to be < 10%, a constant λ underestimates the CBF in the basal ganglia as deep grey matter has lower water content, i.e. lower λ, than cortical GM. Moreover, a λ value estimated for adults may not be appropriate for neonates as neonates have higher water content (Herscovitch and Raichle, 1985). This may lead to globally underestimate the CBF over the brain.

The choice of the longitudinal relaxation time of blood value, T_{1b}, may affect the CBF estimation particularly in neonates who have variable hematocrit values (Varela et al., 2015). (De Vis et al. 2014) demonstrated that the average change in CBF was 11% between perfusion values using an assumed T1b and a corrected T1b. The formula that exists for calculating T1b from each patient's hematocrit (Varela et al., 2011), which is now used in ASL studies in neonates, has been implemented for 3 T magnetic fields. Hematocrit values were available in our population, but we did not find a valid formula at 1.5 T in the literature. We have therefore used an assumed T1b as in most of the other studies. This can overestimate or underestimate CBF values.

For ethical reasons, our study did not have a control group — it is difficult to scan healthy subjects within the first two weeks of their life. Moreover, there was insufficient follow-up in the current study to evaluate the neurodevelopmental prognosis at 2 years. It would be interesting to correlate neurological outcomes with CBF changes during the first 2 weeks of life in a future study, as performed by De Vis et al. on early MRI (De Vis et al., 2015). These authors observed hyperperfusion in the basal ganglia and thalami in 8 children with HIE with a poor neurodevelopmental outcome versus 20 children with HIE who had a good outcome, on MRI performed in the first week of life. These data are promising because the CBF values would thus make it possible to determine a neurodevelopmental prognosis at an early stage, independently of the conventional imaging. The reported cut-off value for CBF was 51 mL/100 g/min in the BGT. When using this cut-off

value, our results were concordant, as median CBF values in the BGT in neonates with abnormal MRI on early MRI were 80.5 [44.3–133.6] mL/100 g/min vs. 43.4 [29.7–87.3] in neonates with normal conventional MRI. However, it could be problematic to use a threshold value given the high inter-subject variability in CBF values as shown in our study and in the literature in healthy children (Avants et al., 2015; Carsin-Vu et al., 2018; Taki et al., 2011) or in neonates (Boudes et al., 2014). As an example, one neonate that presented with a diffuse pattern of injury and died had a CBF value of 44.7 mL/100 g/min in the BGT on early MRI. Conversely, one neonate with no injury on conventional MRI had a CBF value of 93.7 mL/100 g/min in the BGT on early MRI and 14.4 mL/100 g/min on late MRI. In the same way, it would be interesting to determine a cut-off value on late MRI as performed by De Vis et al (2015) on early MRI. Moreover, a cut-off value could also be determined in the cortical grey matter, given that BGT values may not be used as basal perfusion values are not the same, as demonstrated in our results.

In conclusion, we developed a processing pipeline for morphological and ASL data suitable for neonates based on automated segmentation to obtain mean CBF values in ROIs, including the BGT and cortical grey matter. This is a novel approach as the majority of previous studies using ASL in neonates in the literature used manual drawn ROIs. Our study is one of the first to look at changes over time during the first and second week of life on two successive scans. Given that the perfusion differences observed on early MRI between subjects with vs. without injury on MRI were no longer significant on the late scan in our study, ASL sequences in this pathology seem to be more relevant when acquired relatively early, in the first days of life, in line with previous studies and reflecting the reperfusion phenomenon. However, persistent hyperperfusion on late MRI scans in some of our subjects, as also seen in the literature, indicates that this phase may be of inconstant length. The correlation of intra-subject changes in perfusion between early and late MRI with neurodevelopmental outcome warrants investigation in a larger cohort, to determine whether the CBF change pattern can provide additional prognostic information.

References

Agut, T., León, M., Rebollo, M., Muchart, J., Arca, G., Garcia-Alix, A., 2014. Early identification of brain injury in infants with hypoxic ischemic encephalopathy at high risk for severe impairments: accuracy of MRI performed in the first days of life. BMC Pediatr. 14, 177. https://doi.org/10.1186/1471-2431-14-177.

Alderliesten, T., de Vries, L.S., Benders, M.J.N.L., Koopman, C., Groenendaal, F., 2011. MR imaging and outcome of term neonates with perinatal asphyxia: value of diffusion-weighted MR imaging and ^{1}H MR spectroscopy. Radiology 261, 235–242. https://doi.org/10.1148/radiol.11110213.

Alsop, D.C., Detre, J.A., Golay, X., Günther, M., Hendrikse, J., Hernandez-Garcia, L., Lu, H., MacIntosh, B.J., Parkes, L.M., Smits, M., van Osch, M.J.P., Wang, D.J.J., Wong, E.C., Zaharchuk, G., 2015. Recommended implementation of arterial spin-labeled perfusion MRI for clinical applications: a consensus of the ISMRM perfusion study group and the European consortium for ASL in dementia. Magn. Reson. Med. 73, 102–116. https://doi.org/10.1002/mrm.25197.

Avants, B.B., Duda, J.T., Kilroy, E., Krasileva, K., Jann, K., Kandel, B.T., Tustison, N.J.,

Yan, L., Jog, M., Smith, R., Wang, Y., Dapretto, M., Wang, D.J.J., 2015. The pediatric template of brain perfusion. Sci. Data 2, 150003. https://doi.org/10.1038/sdata.2015.3.

Barkovich, A.J., Hajnal, B.L., Vigneron, D., Sola, A., Partridge, J.C., Allen, F., Ferriero, D.M., 1998. Prediction of neuromotor outcome in perinatal asphyxia: evaluation of MR scoring systems. AJNR Am. J. Neuroradiol. 19, 143–149.

Batista, C.E.A., Chugani, H.T., Juhász, C., Behen, M.E., Shankaran, S., 2007. Transient hypermetabolism of the basal ganglia following perinatal hypoxia. Pediatr. Neurol. 36, 330–333. https://doi.org/10.1016/j.pediatrneurol.2007.01.004.

Boudes, E., Gilbert, G., Leppert, I.R., Tan, X., Pike, G.B., Saint-Martin, C., Wintermark, P., 2014. Measurement of brain perfusion in newborns: pulsed arterial spin labeling (PASL) versus pseudo-continuous arterial spin labeling (pCASL). NeuroImage Clin. 6, 126–133. https://doi.org/10.1016/j.nicl.2014.08.010.

Boudes, E., Tan, X., Saint-Martin, C., Shevell, M., Wintermark, P., 2015. MRI obtained during versus after hypothermia in asphyxiated newborns. Arch. Dis. Child. Fetal Neonatal Ed. 100, F238–F242. https://doi.org/10.1136/archdischild-2014-306550.

Buxton, R.B., Frank, L.R., Wong, E.C., Siewert, B., Warach, S., Edelman, R.R., 1998. A general kinetic model for quantitative perfusion imaging with arterial spin labeling. Magn. Reson. Med. 40, 383–396.

Carsin-Vu, A., Corouge, I., Commowick, O., Bouzillé, G., Barillot, C., Ferré, J.-C., Proisy, M., 2018. Measurement of pediatric regional cerebral blood flow from 6 months to 15 years of age in a clinical population. Eur. J. Radiol. 101, 38–44. https://doi.org/10.1016/j.ejrad.2018.02.003.

Chakkarapani, E., Poskitt, K.J., Miller, S.P., Zwicker, J.G., Xu, Q., Wong, D.S.T., Roland, E.H., Hill, A., Chau, V., 2016. Reliability of early magnetic resonance imaging (MRI) and necessity of repeating MRI in noncooled and cooled infants with neonatal encephalopathy. J. Child Neurol. 31, 553–559. https://doi.org/10.1177/0883073815600865.

Charon, V., Proisy, M., Ferré, J.-C., Bruneau, B., Tréguier, C., Beuchée, A., Chauvel, J., Rozel, C., 2015. Comparison of early and late MRI in neonatal hypoxic–ischemic encephalopathy using three assessment methods. Pediatr. Radiol. 45. https://doi.org/10.1007/s00247-015-3419-4.

Cheong, J.L.Y., Cady, E.B., Penrice, J., Wyatt, J.S., Cox, I.J., Robertson, N.J., 2006. Proton MR spectroscopy in neonates with perinatal cerebral hypoxic-ischemic injury: metabolite peak-area ratios, relaxation times, and absolute concentrations. AJNR Am. J. Neuroradiol. 27, 1546–1554.

Commowick, O., Wiest-Daessle, N., Prima, S., 2012a. Block-matching strategies for rigid registration of multimodal medical images. In: Proceedings - International Symposium on Biomedical Imaging, pp. 700–703. https://doi.org/10.1109/ISBI.2012.6235644.

Commowick, O., Wiest-Daesslé, N., Prima, S., 2012b. Automated diffeomorphic registration of anatomical structures with rigid parts: application to dynamic cervical MRI. Med. Image Comput. Comput. Assist. Interv. 15, 163–170.

De Vis, J.B., Petersen, E.T., de Vries, L.S., Groenendaal, F., Kersbergen, K.J., Alderliesten, T., Hendrikse, J., Benders, M.J.N.L., 2013. Regional changes in brain perfusion during brain maturation measured non-invasively with Arterial Spin Labeling MRI in neonates. Eur. J. Radiol. 82, 538–543. https://doi.org/10.1016/j.ejrad.2012.10.013.

De Vis, J.B., Hendrikse, J., Groenendaal, F., de Vries, L.S., Kersbergen, K.J., Benders, M.J.N.L., Petersen, E.T., 2014. Impact of neonate haematocrit variability on the longitudinal relaxation time of blood: Implications for arterial spin labelling MRI. NeuroImage. Clin. 4, 517–525 https://doi.org/10.1016/j.nicl.2014.03.006.

De Vis, J.B., Hendrikse, J., Petersen, E.T., de Vries, L.S., van Bel, F., Alderliesten, T., Negro, S., Groenendaal, F., Benders, M.J.N.L., 2015. Arterial spin-labelling perfusion MRI and outcome in neonates with hypoxic-ischemic encephalopathy. Eur. Radiol. 25, 113–121. https://doi.org/10.1007/s00330-014-3352-1.

Gallichan, D., Jezzard, P., 2009. Variation in the shape of pulsed arterial spin labeling kinetic curves across the healthy human brain and its implications for CBF quantification. Magn. Reson. Med. 61, 686–695. https://doi.org/10.1002/mrm.21886.

Gousias, I.S., Edwards, A.D., Rutherford, M.A., Counsell, S.J., Hajnal, J.V., Rueckert, D., Hammers, A., 2012. Magnetic resonance imaging of the newborn brain: manual segmentation of labelled atlases in term-born and preterm infants. Neuroimage 62, 1499–1509. https://doi.org/10.1016/j.neuroimage.2012.05.083.

Greisen, G., 2014. Cerebral blood flow and oxygenation in infants after birth asphyxia. Clinically useful information? Early Hum. Dev. 90, 703–705. https://doi.org/10.1016/j.earlhumdev.2014.06.007.

Guimond, A., Meunier, J., Thirion, J.-P., 2000. Average brain models: a convergence study. Comput. Vis. Image Underst. 77, 192–210. https://doi.org/10.1006/CVIU.1999.0815.

Herscovitch, P., Raichle, M.E., 1985. What is the correct value for the brain-blood partition coefficient for water? J. Cereb. Blood Flow Metab. 5, 65–69. https://doi.org/10.1038/jcbfm.1985.9.

Kim, H.G., Lee, J.H., Choi, J.W., Han, M., Gho, S.-M., Moon, Y., 2018. Multidelay arterial spin-labeling MRI in neonates and infants: cerebral perfusion changes during brain maturation. AJNR Am. J. Neuroradiol. https://doi.org/10.3174/ajnr.A5774.

Lassen, N.A., 1966. The luxury-perfusion syndrome and its possible relation to acute metabolic acidosis localised within the brain. Lancet 2, 1113–1115.

Luh, W.M., Wong, E.C., Bandettini, P.A., Hyde, J.S., 1999. QUIPSS II with thin-slice TI1 periodic saturation: a method for improving accuracy of quantitative perfusion imaging using pulsed arterial spin labeling. Magn. Reson. Med. 41, 1246–1254.

MacIntosh, B.J., Filippini, N., Chappell, M.A., Woolrich, M.W., Mackay, C.E., Jezzard, P., 2010. Assessment of arterial arrival times derived from multiple inversion time pulsed arterial spin labeling MRI. Magn. Reson. Med. 63, 641–647. https://doi.org/10.1002/mrm.22256.

Massaro, A.N., Bouyssi-Kobar, M., Chang, T., Vezina, L.G., du Plessis, A.J.,

Limperopoulos, C., 2013. Brain perfusion in encephalopathic newborns after therapeutic hypothermia. Am. J. Neuroradiol. 34, 1649–1655. https://doi.org/10.3174/ajnr.A3422.

Maumet, C., Maurel, P., Ferré, J.-C., Barillot, C., 2014. Robust estimation of the cerebral blood flow in arterial spin labelling. Magn. Reson. Imaging 32, 497–504. https://doi.org/10.1016/j.mri.2014.01.016.

Miranda, M.J., Olofsson, K., Sidaros, K., 2006. Noninvasive measurements of regional cerebral perfusion in preterm and term neonates by magnetic resonance arterial spin labeling. Pediatr. Res. 60, 359–363. https://doi.org/10.1203/01.pdr.0000232785.00965.b3.

Ouyang, M., Liu, P., Jeon, T., Chalak, L., Heyne, R., Rollins, N.K., Licht, D.J., Detre, J.A., Roberts, T.P.L., Lu, H., Huang, H., 2017. Heterogeneous increases of regional cerebral blood flow during preterm brain development: preliminary assessment with pseudo-continuous arterial spin labeled perfusion MRI. Neuroimage 147, 233–242. https://doi.org/10.1016/j.neuroimage.2016.12.034.

Petersen, E.T., Zimine, I., Ho, Y.-C.L., Golay, X., 2006. Non-invasive measurement of perfusion: a critical review of arterial spin labelling techniques. Br. J. Radiol. 79, 688–701. https://doi.org/10.1259/bjr/67705974.

Petr, J., Mutsaerts, H.J.M.M., De Vita, E., Steketee, R.M.E., Smits, M., Nederveen, A.J., Hofheinz, F., van den Hoff, J., Asllani, I., 2018. Effects of systematic partial volume errors on the estimation of gray matter cerebral blood flow with arterial spin labeling MRI. Magn. Reson. Mater. Physics, Biol. Med. 31, 725–734. https://doi.org/10.1007/s10334-018-0691-y.

Pienaar, R., Paldino, M.J., Madan, N., Krishnamoorthy, K.S., Alsop, D.C., Dehaes, M., Grant, P.E., 2012. A quantitative method for correlating observations of decreased apparent diffusion coefficient with elevated cerebral blood perfusion in newborns presenting cerebral ischemic insults. Neuroimage 63, 1510–1518. https://doi.org/10.1016/j.neuroimage.2012.07.062.

Proisy, M., Mitra, S., Uria-Avellana, C., Sokolska, M., Robertson, N.J., Le Jeune, F., Ferré, J.-C., 2016. Brain perfusion imaging in neonates: an overview. AJNR Am. J. Neuroradiol. https://doi.org/10.3174/ajnr.A4778.

Pryds, O., Greisen, G., Lou, H., Friis-Hansen, B., 1990. Vasoparalysis associated with brain damage in asphyxiated term infants. J. Pediatr. 117, 119–125.

Rosenbaum, J.L., Almli, C.R., Yundt, K.D., Altman, D.I., Powers, W.J., 1997. Higher neonatal cerebral blood flow correlates with worse childhood neurologic outcome. Neurology 49, 1035–1041.

Saliba, E., Debillon, T., 2010. Hypothermia for hypoxic-ischemic encephalopathy in fullterm newborns. Arch. Pediatr. 17 (Suppl. 3), S67–S77. https://doi.org/10.1016/S0929-693X(10)70904-0.

Serag, A., Aljabar, P., Ball, G., Counsell, S.J., Boardman, J.P., Rutherford, M.A., Edwards, A.D., Hajnal, J.V., Rueckert, D., 2012. Construction of a consistent high-definition spatio-temporal atlas of the developing brain using adaptive kernel regression. Neuroimage 59, 2255–2265. https://doi.org/10.1016/j.neuroimage.2011.09.062.

Skranes, J.H., Cowan, F.M., Stiris, T., Fugelseth, D., Thoresen, M., Server, A., 2015. Brain imaging in cooled encephalopathic neonates does not differ between four and 11 days after birth. Acta Paediatr. 104, 752–758. https://doi.org/10.1111/apa.13016.

Taki, Y., Hashizume, H., Sassa, Y., Takeuchi, H., Wu, K., Asano, M., Asano, K., Fukuda, H., Kawashima, R., 2011. Correlation between gray matter density-adjusted brain perfusion and age using brain MR images of 202 healthy children. Hum. Brain Mapp. 32, 1973–1985. https://doi.org/10.1002/hbm.21163.

Tortora, D., Mattei, P.A., Navarra, R., Panara, V., Salomone, R., Rossi, A., Detre, J.A., Caulo, M., 2017. Prematurity and brain perfusion: arterial spin labeling MRI. NeuroImage Clin 15, 401–407. https://doi.org/10.1016/j.nicl.2017.05.023.

Varela, M., Hajnal, J.V., Petersen, E.T., Golay, X., Merchant, N., Larkman, D.J., 2011. A method for rapid in vivo measurement of blood T1. NMR Biomed. 24, 80–88. https://doi.org/10.1002/nbm.1559.

Varela, M., Petersen, E.T., Golay, X., Hajnal, J.V., 2015. Cerebral blood flow measurements in infants using look-locker arterial spin labeling. J. Magn. Reson. Imaging 41, 1591–1600. https://doi.org/10.1002/jmri.24716.

Volpe, J.J., 2012. Neonatal encephalopathy: an inadequate term for hypoxic-ischemic encephalopathy. Ann. Neurol. 72, 156–166. https://doi.org/10.1002/ana.23647.

Wang, J., Licht, D.J., 2006. Pediatric perfusion MR imaging using arterial spin labeling. Neuroimaging Clin. N. Am. 16, 149–167. https://doi.org/10.1016/j.nic.2005.10.002.

Wang, J., Licht, D.J., Silvestre, D.W., Detre, J.A., 2006. Why perfusion in neonates with congenital heart defects is negative—technical issues related to pulsed arterial spin labeling. Magn. Reson. Imaging 24, 249–254. https://doi.org/10.1016/j.mri.2005.10.031.

Watson, C.G., Dehaes, M., Gagoski, B.A., Grant, P.E., Rivkin, M.J., 2016. Arterial spin labeling perfusion magnetic resonance imaging performed in acute perinatal stroke reveals hyperperfusion associated with ischemic injury. Stroke 47, 1514–1519. https://doi.org/10.1161/STROKEAHA.115.011936.

Wintermark, P., Moessinger, A.C., Gudinchet, F., Meuli, R., 2008. Temporal evolution of MR perfusion in neonatal hypoxic-ischemic encephalopathy. J. Magn. Reson. Imaging 27, 1229–1234. https://doi.org/10.1002/jmri.21379.

Wintermark, P., Hansen, A., Gregas, M.C., Soul, J., Labrecque, M., Robertson, R.L., Warfield, S.K., 2011. Brain perfusion in asphyxiated newborns treated with therapeutic hypothermia. Am. J. Neuroradiol. 32, 2023–2029. https://doi.org/10.3174/ajnr.A2708.

Wintermark, P., Hansen, A., Warfield, S.K., Dukhovny, D., Soul, J.S., 2014. Near-infrared spectroscopy versus magnetic resonance imaging to study brain perfusion in newborns with hypoxic-ischemic encephalopathy treated with hypothermia. Neuroimage 85 (Pt 1), 287–293. https://doi.org/10.1016/j.neuroimage.2013.04.072.

Wong, E.C., Buxton, R.B., Frank, L.R., 1998. Quantitative imaging of perfusion using a single subtraction (QUIPSS and QUIPSS II). Magn. Reson. Med. 39, 702–708.